BUTTERWORTH HEINEMANN

Polymer Vol. 36 No. 6, pp. 1189–1198, 1995

0032-3861/95/$10.00+0.00

Effects of the distributions of polypropylene fibre properties on the tensile response of fibre assemblies

Erik Andreassen* and Einar L. Hinrichsen
Sintef, PO Box 124 Blindern, N-0314 Oslo, Norway

and Kristin Grøstad, Ole Jan Myhre and Marianne D. Braathen
Borealis, N-3960 Stathelle, Norway
(Received 18 March 1994; revised 28 June 1994)

The tensile response of some simple fibre assemblies is calculated, using the actual stress–strain relationships of constituent fibres. These stress–strain relationships are obtained by a scaling procedure, with distributions of ultimate tensile properties and an average stress–strain curve as input. Two polypropylene fibres with different polydispersity index, but the same weight-average molecular weight and draw ratio, are considered in this article. The fibre with the narrowest molecular weight distribution (*MWD*) has about 30% higher average strength. On the other hand, if bundles with a large number of fibres are compared, the strength of a bundle consisting of fibres with narrow *MWD* is less than 10% higher. The maximum strength of a random planar distribution of fibres is 36% and 44% of the average fibre strength, for fibres with narrow and broad *MWD*, respectively. The strength of a chain-of-bundles decreases as the number of bundles increases, and as the number of fibres in each bundle decreases. When the number of bundles is large, the strength of a chain-of-bundles containing fibres with broad *MWD* exceeds that of a chain containing fibres with narrow *MWD*. The assemblies considered in this article illustrate effects in real assemblies, such as non-woven fabrics. They also provide references for the tensile properties of real assemblies.

(Keywords: polypropylene; fibres; tensile properties)

INTRODUCTION

The literature on the tensile properties of fibres is mainly concerned with the average values of characteristics such as the tensile modulus, the elongation at break and the tensile strength. In some studies more information is extracted from the stress–strain curves, e.g. by identifying characteristic points using derivative analysis[1]. Stress–strain curves in the literature are either selected as representative for the parallels tested, or obtained from all the parallels by an averaging procedure.

The tensile response of fibre assemblies, such as yarns and fabrics, can of course be quite different from the average stress–strain curve of the constituent fibres. The tensile response of fibre assemblies depends on the distribution of tensile properties among the constituent fibres, the fibre configuration, and the interaction between fibres. Polymer composites can be thought of as fibre assemblies embedded in a matrix, and effects of the variability in fibre strength on the strength of composities is an area of active research.

The literature on distributions of tensile properties for synthetic polymer fibres is scarce. Pompo *et al.*[2] showed that the elongation and stress at break for poly(ethylene terephthalate) fibres were distributed according to Weibull statistics, and they correlated the Weibull parameters to the process and to the fibre morphology. Amornsakchai *et al.*[3] observed a broadening of the distribution of stress at break with increasing draw ratio for polyethylene fibres. Tsai[4] reported that the widths of the distributions of elongation and stress at break for modacrylic fibres could be varied independently by adjusting material and processing parameters.

A bundle of fibres is perhaps the most simple fibre assembly. A large number of theoretical publications deal with the statistical properties of the strength of bundles, with various assumptions and modifications[4–13]. Analytical expressions for the strength of bundles with an infinite number of filaments have also been derived in these papers. However, the stress–strain relationship of the constituent filaments is stated in a general or idealized (usually Hookean) form.

Numerical simulations have been performed for the tensile deformation and failure of two-dimensional fibre assemblies, i.e. fabrics. Boyce *et al.*[14] presented a model for a woven fabric, consisting of a grid of unit cells of length equal to the repeat unit of the weave. The strength distribution of the yarn was used as input to the model. Different mechanisms for the local load redistribution subsequent to a break were studied. Britton *et al.*[15–17] developed a computer model for the tensile deformation of a point-bonded non-woven fabric, based on a microscopic description. In this model, the fabric consisted of

* To whom correspondence should be addressed

a collection of straight Hookean fibres of finite length, laid down randomly with respect to position and orientation. The intersection of any two fibre segments represented a possible bonding site. Intersections to be bonded were selected randomly and given a strength, randomly selected from a distribution function. Grindstaff and Hansen[18] developed a somewhat more realistic model for a non-woven fabric, by including parameters such as bond layout, fabric density, orientation and curl of fibres, and tensile properties of bonds and fibres. Stress–strain relationships for the fibres were average values. However, Grindstaff and Hansen, contrary to Britton *et al.*, assumed uniform local elongation. Some of these simulated tensile responses have been compared with experimental data, and the agreement is claimed to be good. However, in order to optimize the fibre properties, we feel that a more exact representation of the tensile response of single fibres is needed in simulations of this kind.

This article consists of four main sections. In the first section some results from the tensile testing of two polypropylene fibres are presented. These two fibres have different shapes of the stress–strain curves, and different distributions of ultimate tensile properties. In the second section a model for the tensile response of a fibre bundle is presented. The input to the model is obtained from the mechanical data reported in the first section. Our model differs from those mentioned above by using the entire stress–strain curve of each constituent fibre. The basic elements of this model can be used in models for other fibre assemblies as well—some examples of this are given in the last two sections.

THE DISTRIBUTION OF TENSILE PROPERTIES FOR SINGLE FIBRES

In an earlier study[19], the effects of processing parameters and molecular weight distribution (*MWD*) on the tensile properties of polypropylene (PP) fibres were investigated. In this article we will focus on two of the fibres from this earlier work, and their distributions of tensile properties. The fibres were produced in a short-spin process consisting of three integrated stages (spinning, drawing and annealing). Their linear density is 4 dtex (0.4 g km^{-1}) and the draw ratio is 3. The difference between the two fibres is the width of the *MWD*. The weight-average molecular weight is the same. Hence, the fibres will be denoted FB (broad *MWD*, $M_w/M_n \sim 5$) and FN (narrow *MWD*, $M_w/M_n \sim 3$). For each fibre 120 parallels were tested. Additional experimental details can be found in ref. 19.

'Average' stress–strain curves were produced by the following procedure. (1) Average values of elongation at break (ε_b) and tenacity at break (σ_b) were calculated. (The nominal stress of fibres, i.e. load divided by initial cross-section, is usually given in the units N tex^{-1}, and called tenacity. The cross-sectional area is equal to the ratio of linear density to bulk density. Hence, 1 cN tex^{-1} corresponds to 10ρ MPa, where ρ is the bulk density measured in g cm^{-3}. In this article, elongation is defined as relative extension.) (2) The stress–strain curve of each parallel was scaled by multiplicative factors, in order to end at the point (ε_b, σ_b) given by the average values. (3) The average curve was calculated from the scaled curves. For most fibres, this average stress–strain curve represents the average fibre response well. Average stress–strain curves for fibres FB and FN are shown in *Figure 1*. These fibres have almost the same average elongation at break, but fibre FN has 29% higher average tenacity at break. The effect of *MWD* on the stress–strain curves has been discussed earlier[19].

Figures 2 and *3* show tenacity at break vs. elongation at break for the parallels of the two fibres. In *Figure 3* the correlation is very low, while the correlation coefficient for the data in *Figure 2* has the value −0.9. The *MWD* trends in *Figures 2* and *3* are observed for all fibres with draw ratio 3. For a draw ratio of 1.5, the correlation coefficients of broad and narrow *MWD* fibres differ less; on the average the former are slightly positive, while the latter are slightly negative. The width of the distribution of tenacity at break is almost independent of the elongation at break in *Figure 2*, while it seems to decrease with increasing elongation at break in *Figure 3*.

The correlation coefficient for the average values of elongation and tenacity at break, for the whole range of fibres studied[19], is about −0.9. If only variations in processing parameters are considered, this correlation coefficient is very close to −1. It is well known that a change in processing parameters which leads to a higher

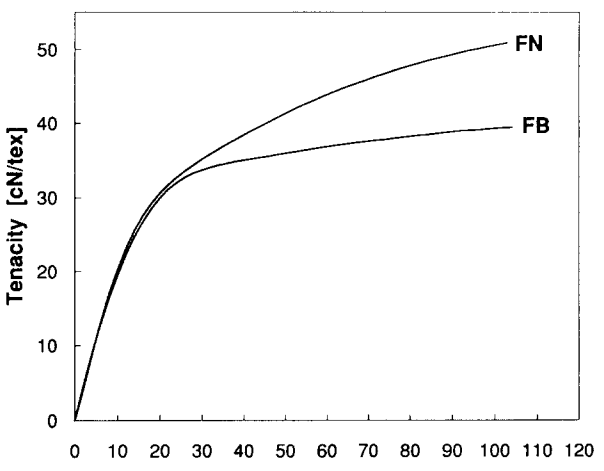

Figure 1 Average stress–strain curves of fibres FN and FB

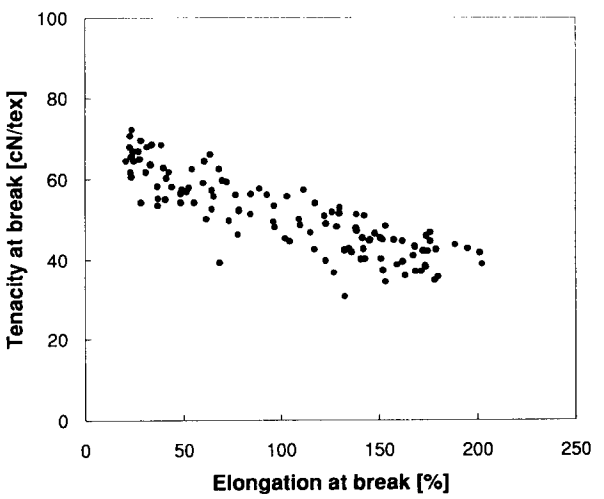

Figure 2 Tenacity at break vs. elongation at break for 120 parallels of fibre FN

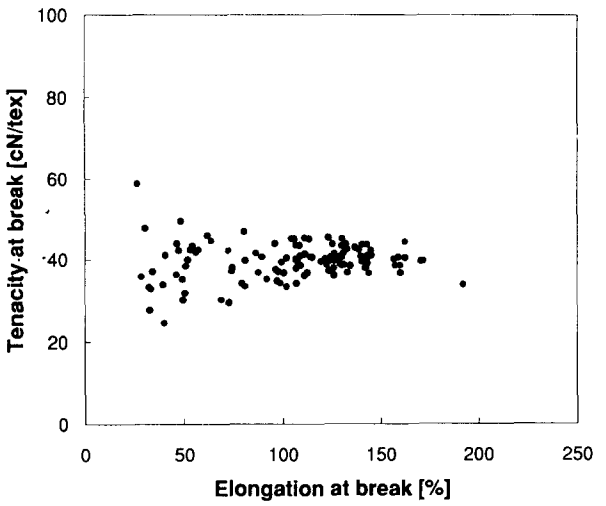

Figure 3 Tenacity at break vs. elongation at break for 120 parallels of fibre FB

average strength also leads to a lower average elongation at break.

The data in *Figures 2* and *3* can be considered as samples from two-dimensional (2D) probability distribution functions (*PDF*s), $p(\varepsilon_b, \sigma_b)$. Hence,

$$p(\varepsilon_b, \sigma_b)\, d\varepsilon_b\, d\sigma_b \tag{1}$$

is the probability that a fibre has elongation at break between ε_b and $\varepsilon_b + d\varepsilon_b$, and tenacity at break between σ_b and $\sigma_b + d\sigma_b$. In order to model the response of fibre assemblies, we must quantify the *PDF*s. Our data set is too small for a full 2D function fitting or spline generation. Hence, we have chosen a simpler approach, which, as we will show in the next section, produces satisfactory results.

Assume that the *PDF* can be written as a product of two independent distributions

$$p = q(\zeta) r(\xi) \tag{2}$$

For fibre FB we simply set $\zeta = \varepsilon_b$ and $\xi = \sigma_b$. For fibre FN we rotate the axes until the correlation coefficient is zero. Hence,

$$\zeta = \varepsilon_b \cos\omega + \sigma_b \sin\omega \tag{3a}$$

$$\xi = -\varepsilon_b \sin\omega + \sigma_b \cos\omega \tag{3b}$$

where ω is the rotation angle. This transformation is not formally correct, since the *PDF* is not generally normalized in the first quadrant of both the original and the rotated coordinate system. However, for the distributions in this study the difference can be neglected. The *PDF* can now be determined by fitting the continuous cumulative distribution functions (*CDF*s)

$$Q(\zeta) = \int_0^{\infty}\int_0^{\zeta} p(\zeta', \xi')\, d\zeta' d\xi' = \int_0^{\zeta} q(\zeta')\, d\zeta' \tag{4a}$$

$$R(\xi) = \int_0^{\xi}\int_0^{\infty} p(\zeta', \xi')\, d\zeta' d\xi' = \int_0^{\xi} r(\xi')\, d\xi' \tag{4b}$$

to experimental data. We have tried to use as simple *CDF*s as possible. A two-parameter Weibull distribution is used for $R(\xi)$ (corresponding to tenacity at break):

$$R(\xi) = 1 - \exp(-(\xi/\alpha)^{\beta}) \tag{5}$$

This *CDF* is often applied to brittle fibres. However, the plots in *Figure 4* show that it can be applied to our PP fibres as well. A slightly better overall fit is obtained with a three-parameter Weibull distribution, but the tails of the distributions are better described by equation (5). Some alternative functions, including the integral of a Gauss function, have also been considered, but none of these fit the data significantly better than a two-parameter Weibull distribution.

The coefficient of variation (*CV*) of the fibre strength is often quoted when assessing the mechanical properties of fibres. The *CV* value depends on the type of spinning process, processing conditions and material parameters. If *CV* is calculated from the 120 parallels, fibre FB has *CV* = 12%. Alternatively, *CV* can be calculated from the Weibull *PDF*. This leads to

$$CV = \left(\frac{\Gamma(1+2/\beta)}{\Gamma^2(1+1/\beta)} - 1\right)^{1/2} \tag{6}$$

where $\Gamma(\,)$ is the Gamma function. Using equation (6), a *CV* value of 11% is obtained for fibre FB. Hence, this Weibull distribution describes the width of the distribution well.

The data corresponding to elongation at break seem to have two regimes. For low ζ values the distributions have no tails. The following function fits the data well:

$$Q(\zeta) = \begin{cases} 0 & \text{for } \zeta < \zeta_0 \\ A + B\sqrt{\zeta} & \text{for } \zeta_0 < \zeta < \zeta_{trans} \\ [C - \exp(-(\zeta/\alpha)^{\beta})]/C & \text{for } \zeta > \zeta_{trans} \end{cases} \tag{7}$$

with $\zeta_0 = (A/B)^2$. $Q(\zeta)$ and its derivative should be continuous functions. This reduces the number of independent parameters in equation (7) to four, e.g. α, β, ζ_{trans} and C. Experimental data and fitted functions are shown in *Figure 5*. Note that $q(\zeta)$, and hence $p(\varepsilon_b, \sigma_b)$, generally will have two local maxima; at $\zeta = \zeta_0$ and

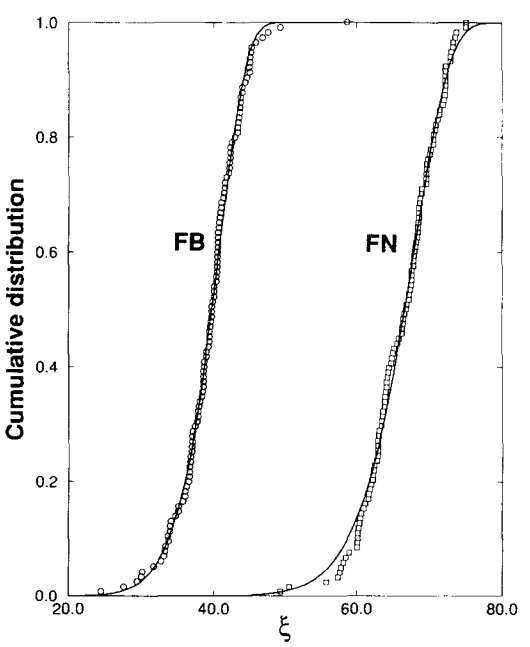

Figure 4 Cumulative distributions of transformed tenacity at break. Experimental data are shown as symbols, fitted functions as solid lines. The fitted parameters are $\alpha = 68.2$ and $\beta = 15.0$ for fibre FN, and $\alpha = 41.0$ and $\beta = 11.6$ for fibre FB

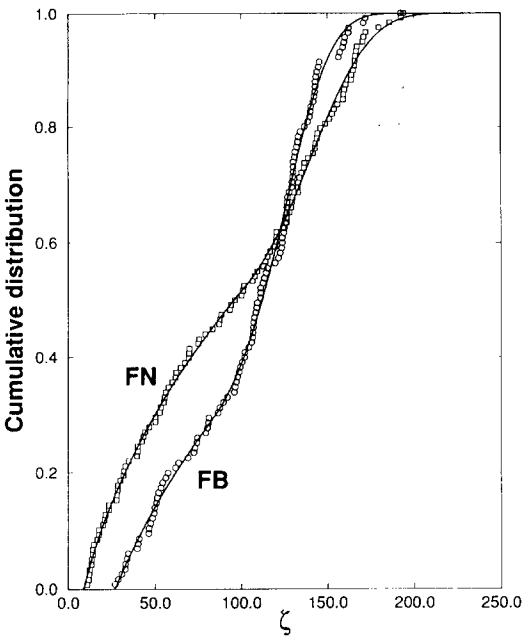

Figure 5 Cumulative distributions of transformed elongation at break. Experimental data are shown as symbols, fitted functions as solid lines

$\zeta = \alpha((\beta-1)/\beta)^{1/\beta}$. Multimodal distributions of ultimate mechanical properties indicate that the failure is controlled by several defect distributions. Dimitrova *et al.*[20], for instance, recently reported distributions of elongation and stress at break with several maxima, for PP films.

THE TENSILE RESPONSE OF AN IDEAL BUNDLE OF FIBRES

Consider a bundle consisting of an infinite number of parallel non-interacting fibres which are clamped at both ends and deformed at a constant elongation rate. For this bundle, tenacity vs. elongation can be expressed as

$$\sigma(\varepsilon) = c(\varepsilon) \int_{\varepsilon}^{\infty} \int_{0}^{\infty} \sigma_f(\varepsilon; \varepsilon_b, \sigma_b)\, q(\zeta(\varepsilon_b, \sigma_b))\, r(\xi(\varepsilon_b, \sigma_b))\, d\sigma_b d\varepsilon_b \tag{8}$$

In this equation, $q(\zeta)$ and $r(\xi)$ are the two functions which constitute the 2D fracture *PDF* described above. Furthermore, $\sigma_f(\varepsilon; \varepsilon_b, \sigma_b)$ is the tenacity at elongation ε for the average curve (defined in the preceding section), after it has been scaled to end at $(\varepsilon_b, \sigma_b)$. This representation, with the average stress–strain curve and the fracture *PDF* decoupled, will be used in all subsequent sections. Of course, equation (8) will not represent the true tensile response of an infinite number of fibres as long as its input is based on a finite number of parallels. However, 120 parallels is sufficient for the comparisons between assemblies of fibres FN and FB that will be made in this article.

The weakness of the simple scaling procedure which was outlined in the preceding section is that the yield elongation of reconstructed curves is incorrect. A more complicated scaling procedure would remedy this, but the correction factors, $c(\varepsilon)$, shown in *Figure 6* have the same effect. The prefactor corrects for imperfections in the scaled average curves. It is simply the ratio of the sum of 120 parallels to the sum of 120 'reconstructed' parallels (each scaled from the average curve so that its endpoint matches the measured ultimate tensile properties) for a given elongation.

Stress–strain curves calculated with equation (8) are shown in *Figure 7*. In equation (8) and all the other models in this article, the elongation is the independent variable. If effects of the deformation/loading rate are neglected, the tensile response up to the maximum tenacity would be the same if the load was the independent variable. Hence, the maximum bundle tenacity is equivalent to the bundle strength. The energy to break will of course depend on the choice of the independent variable, when the stress–strain curve with elongation as independent variable decreases towards zero as in *Figure 7*.

The normalized sum of the 120 measured stress–strain parallels is also plotted in *Figure 7* (the sum is divided by 120, in order to get the nominal stress). As expected, these curves closely follow the calculated curves, since the latter are based on data from the former. This is also an indirect verification of the assumption above, that the fracture *PDF* can be split into two independent functions. In *Figure 7* the maximum tenacity of the bundle containing fibre FN is 8% higher than that containing fibre FB, while the average tenacity at break of fibre FN is 29% higher (*Figure 1*). The ratio of bundle strength to average fibre strength is 77% and 92% for fibres FN and FB, respectively.

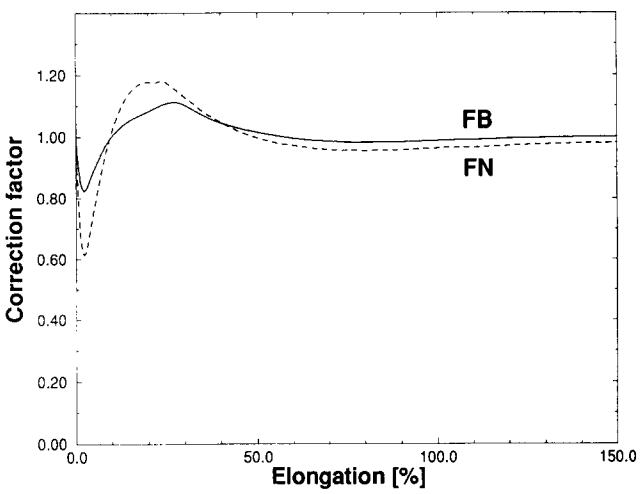

Figure 6 Correction factors, $c(\varepsilon)$

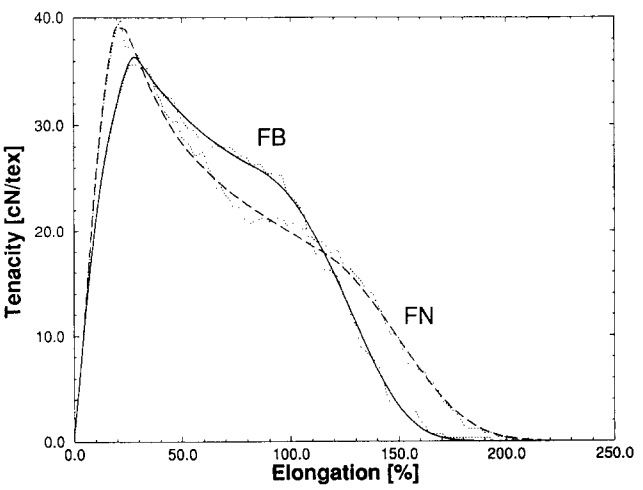

Figure 7 Stress–strain curves calculated for infinite bundles of FB and FN fibres. Normalized sums of 120 parallels are shown as dotted lines

The maximum tenacity of the FB bundle occurs at $\varepsilon = 28.1\%$, which is just after the breaking of the first fibre at $\varepsilon = \zeta_0 = 26.7\%$ (this is also a local maximum of the fracture *PDF*). According to the fracture *PDF*, the first fibre in the FN bundle breaks at $\varepsilon = 8.9\%$, but, since $\omega \neq 0$, the low-elongation maximum of the fracture *PDF* is at a higher elongation, namely $\varepsilon = 19.5\%$. *Figure 7* shows that the maximum tenacity of the FN bundle occurs at an elongation just above this.

The fraction of unbroken fibres at a given elongation can be calculated by integrating the product of $q(\zeta)$ and $r(\xi)$ as in equation (8). Results for fibres FB and FN are shown in *Figure 8*. A comparison of *Figures 7* and *8* shows that at high elongations the tensile response of the bundle is mainly determined by the *PDF*. However, at lower elongations, the bundle strength depends on both the *PDF* and the shape of the stress–strain curves of the constituent fibres. This is illustrated in *Figure 9*, in which 'mixed' input is used in equation (8) (the average stress–strain curve of fibre FB is scaled according to the fracture *PDF* of fibre FN, and vice versa). The highest bundle strength is achieved when the average curve is that of fibre FB and the *PDF* is that of fibre FN. This is because the stress–strain curves of FB fibres have a plateau with tenacity almost as high as the tenacity at break, while FN fibres have a higher level of tenacity at break. The tensile responses of the bundles in *Figure 9* are independent of the shape of the stress–strain curves of the constituent fibres at elongations above ~150%.

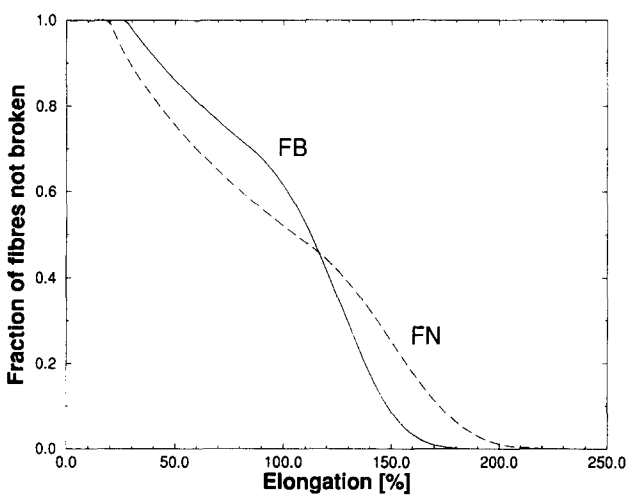

Figure 8 Calculated fraction of fibres not broken in an infinite bundle vs. elongation

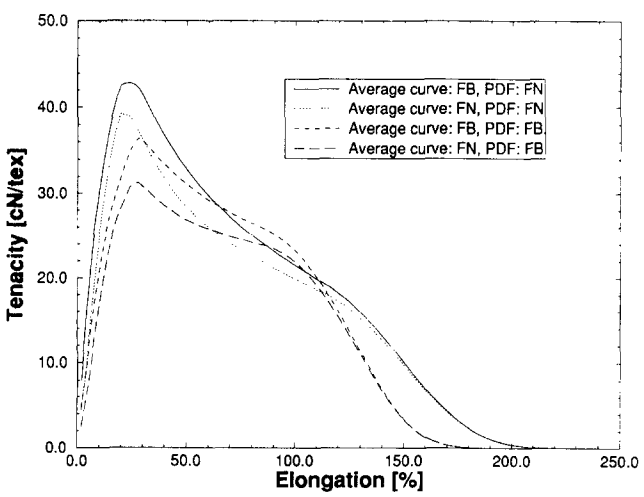

Figure 9 Stress–strain curves calculated with equation (8) using mixed input (see text for explanation)

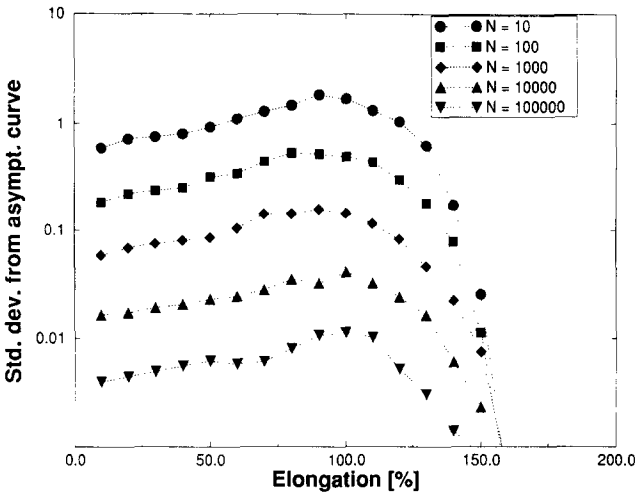

Figure 10 Standard deviation from the asymptotic stress–strain curve for 100 parallels of bundles containing N fibres. Input to the calculation is based on fibre FB, but the *PDF* is simplified to a product of two Weibull distributions

The model described above can of course be modified for the modelling of bundles consisting of a finite number of fibres: N sets of $(\varepsilon_b, \sigma_b)$ are selected using the *PDF*, and the integrals in equation (8) are replaced by sums. The difference between the stress–strain curves of finite and infinite (asymptotic) bundles can be assessed by calculating the standard deviation from asymptotic behaviour for a large number of bundles, each containing N fibres. An example of this is shown in *Figure 10*, in which this standard deviation is plotted vs. elongation. The standard deviation has a maximum vs. elongation which coincides with the average elongation at break. For a given elongation, the standard deviation decreases as the inverse square root of N. This behaviour was expected from statistical theory[12]. The relative standard deviation (standard deviation from asymptotic tenacity divided by asymptotic tenacity) increases monotonically with increasing elongation for elongations above 10–20%.

Stress–strain curves for some real bundles of parallel FB and FN type fibres are shown in *Figure 11*. The main differences compared to *Figure 7* are the maximum values, and the plateau for the FB bundle in *Figure 11*. The bundles are not tested with the same instrument as single fibres. Hence, the higher maximum values in *Figure 11* are probably due to different transducer calibrations (slack in the bundle would have caused the opposite effect). The breaking of fibres seems to be 'delayed' at the plateau for fibre FB in *Figure 11*. This might be because the two fibres have different tendencies for necking[19]. When single fibres are tested, necks are usually initiated at the clamps. The clamping force on fibres inside a bundle will be more evenly distributed. Hence, necks will not be so easily initiated.

The testing of single fibres is tedious and time consuming. Lienkamp and Exner[21] recently presented a method for obtaining the fracture strength distribution of Hookean fibres from a bundle test. Bundle tests could also be useful for non-Hookean fibres, but the differences between *Figures 7* and *11* require further studies.

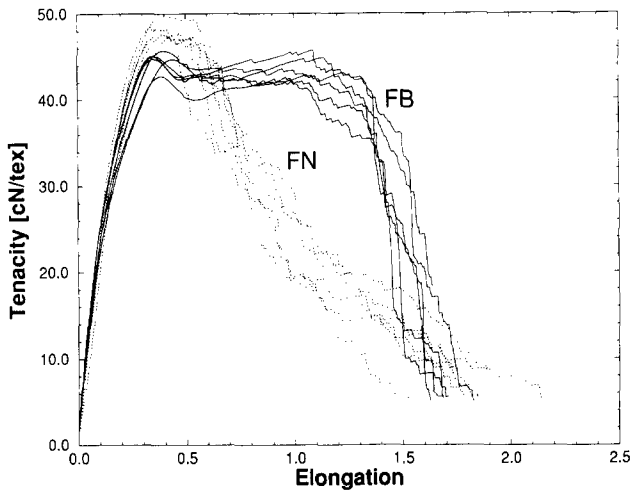

Figure 11 Experimental results from the testing of bundles containing 100 fibres. Six parallels are shown for each type of fibre. The elongation rate is the same as for the testing of single fibres

THE TENSILE RESPONSE OF AN IDEAL PLANAR DISTRIBUTION OF FIBRES

Consider a planar distribution consisting of an infinite number of straight non-interacting fibres, from which a rectangular section with aspect ratio $\Re = w/l_o$ is subjected to uniaxial deformation (*Figure 12*). Furthermore, we assume that the fibres are infinitely long.

The elongation rate experienced by a given fibre depends on the angle θ between the fibre and the testing direction. Samuels[22] studied the effect of the elongation rate on the distribution of true stress at break for PP films. In general, the average tenacity at break will decrease with decreasing elongation rate (increasing θ), while the average elongation at break will increase. The fracture *PDF* is also affected by the initial length of a fibre ($l_{fo} = l_o/\cos\theta_o$ in *Figure 12*)[23].

If rate and length effects are neglected, the tensile response of the rectangular sample can be expressed as

$$\sigma(\varepsilon) = \int_0^{\theta_o^*} \Psi(\theta_o)\,\Omega(\theta_o, \Re)\cos\theta\, I_f\, d\theta_o \qquad (9)$$

with

$$I_f = c(\varepsilon_f)\int_{\varepsilon_f}^{\infty}\int_0^{\infty} \sigma_f(\varepsilon_f; \varepsilon_b, \sigma_b)\, p(\varepsilon_b, \sigma_b)\, d\sigma_b d\varepsilon_b \qquad (10)$$

The planar distribution of fibres is assumed to be symmetrical about the testing direction. Hence, the integral in equation (9) extends from zero to the cut-off angle

$$\theta_o^* = \arctan \Re \qquad (11)$$

since fibres with initial angle θ_o above θ_o^* are not clamped at both ends. Referring to *Figure 12*, the global elongation of the sample is

$$\varepsilon = \frac{l - l_o}{l_o} \qquad (12)$$

The elongation of a fibre initially at an angle θ_o to the testing direction is

$$\varepsilon_f(\theta_o, \varepsilon) = \frac{l_f - l_{fo}}{l_{fo}} \qquad (13)$$

Local elongations ε_f that are used in equation (10) are calculated from the global elongation ε and the initial angle θ_o, using simple geometric considerations:

$$l_o = l_{fo}\cos\theta_o \qquad (14)$$

and

$$l_f^2 = l_{fo}^2 \sin^2\theta_o + l^2 \qquad (15)$$

The fibre orientation distribution function (*ODF*), $\Psi(\theta_o)$, is normalized on the interval $[0, \theta_o^*]$. This is because only fibres with θ_o in this interval are part of the cross-section that is being tested. Note that equation (9) is reduced to equation (8) when the orientation distribution is a Dirac delta function:

$$\Psi(\theta_o) = \delta(0) \qquad (16)$$

A random planar distribution of fibres is represented by

$$\Psi(\theta_o) = 1/\theta_o^* \qquad (17)$$

The next function in equation (9) is the 'window' function

$$\Omega(\theta_o, \Re) = \cos\theta_o - \Re^{-1}\sin\theta_o, \qquad \theta_o \in [0, \theta_o^*] \qquad (18)$$

which is equal to the normalized number of fibres, with initial angle θ_o, that contribute to the stress–strain curve

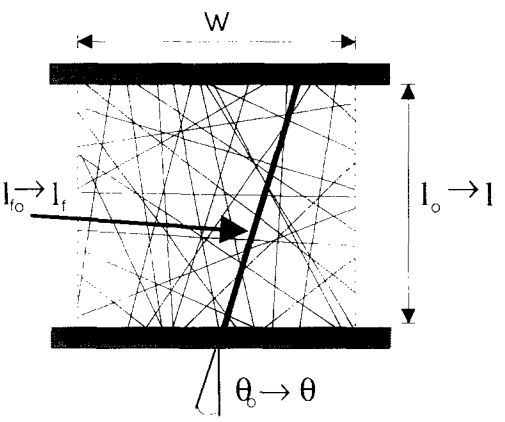

Figure 12 Schematic illustration of the tensile testing of a rectangular sample of a planar distribution of fibres

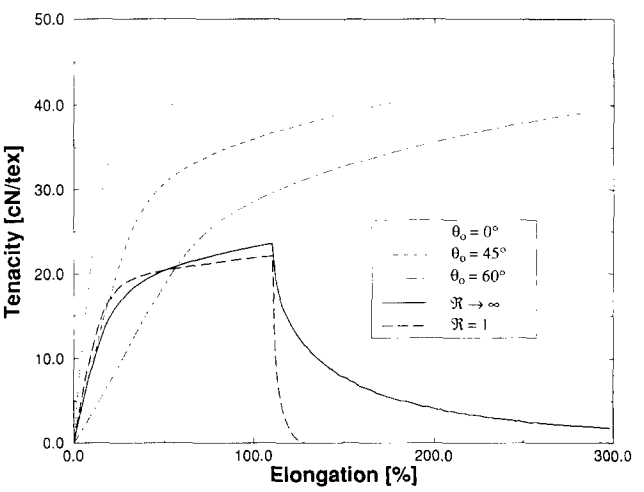

Figure 13 Calculated stress–strain curves for single fibres 'mounted' at 0°, 45° and 60° to the testing direction, and for samples of random planar distributions of the same fibre. In order to illustrate the effect of the *ODF*, the fracture *PDF* is a Dirac delta function

of the rectangular sample. I_f given by equation (10) is analogous to equation (8) and represents the tenacity of fibres with initial angle θ_0. Since only the load component in the testing direction is measured, equation (9) contains a $\cos\theta$ factor.

Some characteristics of the tensile response of random planar distributions are illustrated in *Figure 13*. In order to separate the effects of the fracture *PDF* and the *ODF*, the former is a Dirac delta function (independent of local elongation rates and initial fibre lengths) in this figure, i.e. all fibres have the same stress–strain curve. Calculated stress–strain curves of single fibres 'mounted' at different angles to the testing direction are also shown in *Figure 13*. At low elongations, the stress–strain curve of a random planar distribution with infinite aspect ratio follows that of a single fibre mounted at an angle 45° to the testing direction.

The limiting behaviour of a random planar distribution of identical Hookean fibres, with an infinite aspect ratio, can be calculated. It is easy to show that the ratio of maximum assembly tenacity to tenacity at break of constituent fibres approaches 3/8 (0.375) in the limit $\varepsilon_b \to 0$. (The apparent tensile modulus ($\varepsilon \to 0$) of a single Hookean fibre mounted at an angle 45° to the testing direction is $2\sqrt{2}/8 (\approx 0.354)$ times the actual tensile modulus of the fibre.) This ratio increases with increasing ε_b. For $\varepsilon_b = 500\%$ it is close to 0.5.

Stress–strain curves of random planar distributions of fibres FB and FN, calculated by equation (9), are shown in *Figure 14*. The aspect ratio ($\Re$) is 10 in this figure. The effect of initial fibre lengths is estimated by using the expression suggested by Boyce *et al.*[14] for the fracture *CDF*:

$$1 - \exp\left[-\frac{l_{fo}}{l_t}\left(\frac{x}{\alpha}\right)^{\beta} \right] \qquad (19)$$

where l_t is the initial gauge length that was used when single fibres were tested. For $R(\xi)$ (equation (4b)) this modification is straightforward. For $Q(\zeta)$ (equation (4a)) the Weibull regime is modified according to the expression above (Boyce *et al.* did not consider the distribution of elongation at break), and the parameters A and B are adjusted for each l_{fo} to ensure that $Q(\zeta)$ and its derivative are continuous functions. *Figure 14* shows that the effect of this modification of the fracture *PDF* is small. The strength of the assemblies will not be significantly affected by either rate or length effects, since only fibres that are almost parallel to the testing direction will break before the elongation at maximum tenacity is reached.

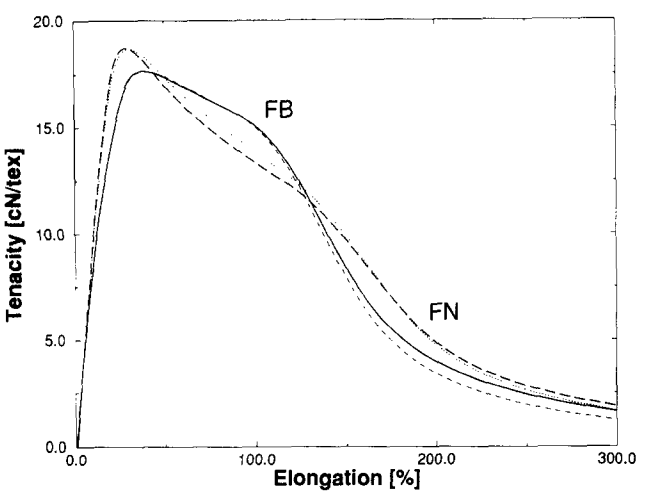

Figure 14 Calculated stress–strain curves for random planar distributions of fibres FB and FN. — (FB) and – – – (FN): effects of local deformation rates and initial lengths are neglected. ---- (FB) and ····· (FN): effects of the initial length of the fibre are included, as described by equation (19)

The main difference between *Figure 7* (bundles) and *Figure 14* (random planar distributions) was expected: the latter type of assembly has a lower strength, but its stress–strain curve has a longer tail at high elongations. The ratio of fibre FN assembly strength to fibre FB assembly strength is about the same in *Figures 7* and *14*. This is because the maxima in *Figure 14* correspond to the breaking of the first fibres, which are parallel to the testing direction.

The simple model described above can supply references (upper limits) for the ratio of non-woven fabric strength to fibre strength. This model also gives some information about the initial stiffness of the fabric—the stress–strain curve of a non-woven, before the first local failure, mainly derives from the geometrical arrangement of the fibres. The nominal stress of fabrics is recorded as load divided by gauge width. For single fibres, and for the models above, the unit is load divided by linear density. The linear density of a fabric (in the testing direction) is the product of areal density and gauge width. All fibres contribute to the areal density. Hence, the *ODF* in equation (17) should be normalized on the interval $[0, \pi/2]$ when comparing results from this model with experimental data.

When a real non-woven is tested, according to standard procedures, the gauge length usually exceeds the fibre length. Hence, there are no fibres that are clamped at both ends, and the effect of the sample aspect ratio ($\Re$), as described above, will not be present. Above a certain 'network' threshold, all the fibres that are clamped contribute to the tensile response of the fabric. Edge effects will affect the measured strength—failure is preferentially initiated at the unclamped edge. Warner[24] measured the strength of a non-woven for $\Re = 0.5$, 0.2 and 0.1 (the gauge length was 10 cm in all cases). The strength and the elongation at break of the fabric decreased with decreasing $\Re$.

The ratio of asymptotic assembly strength to average fibre strength, predicted by equation (9) with infinite $\Re$, is an upper limit for the ratio of non-woven strength to average fibre strength. For a random planar distribution, neglecting effects of different elongation rates and initial fibre lengths, this upper limit is 36% and 44% for fibres FN and FB, respectively. Real values of this ratio will be lower due to the network structure of the non-woven and imperfect fibre–fibre bonds. Non-wovens are usually anisotropic with the highest strength in the machine direction (MD). For commercial thermally bonded PP non-wovens, a typical value for the ratio of non-woven MD strength to average fibre strength is about 30%.

The description of the stress–strain relationships of constituent fibres, which was used in this and the preceding section, can be implemented in a microscopic model of a non-woven fabric. An example of such a model is that of Grindstaff and Hansen[18] (cf. Introduction), featuring finite fibre lengths and a realistic layout of fibres and bonds. The weak point of such models is the

assignment of bond properties. Different mechanisms can cause fracture of non-woven fabrics, depending on the fibre properties and the processing of the fabric. The fracture of thermally bonded non-woven fabrics is usually initiated by the breaking of fibres at the perimeter of the bond spots, or by the disintegration of bond spots. The bond spots can disintegrate into large pieces or single fibres. The mechanical properties of the bonds could be evaluated by comparing simulated and measured non-woven stress–strain curves, with realistic input for the microscopic geometry and the stress–strain relationship of fibres. Hence, the contributions of fibres and bonds to the tensile response of the non-woven could be isolated. This would be helpful in the interpretation of tensile data of non-wovens. The data published by Wei *et al.*[25] could, for instance, be analysed in this way. Wei *et al.* measured the tenacity and elongation at break of thermally bonded PP non-wovens. The former increased with increasing bonding temperature for all the fibres that were used in the study. The elongation at break also increased with increasing bonding temperature for fibres with low draw ratios, while the opposite effect was observed for fibres with high draw ratios.

THE TENSILE RESPONSE OF A CHAIN-OF-BUNDLES

The tensile response of the assemblies in the two preceding sections could be expressed as integrals (infinite assemblies) or sums (finite assemblies), since all fibres were loaded in parallel. Real assemblies usually include serial elements. A simple one-dimensional assembly of this kind is the chain-of-bundles[12,26], which consists of K bundles arranged in series. Each bundle contains N fibres.

The tensile response, $\sigma(\varepsilon)$, of this assembly can be calculated by a relaxation procedure. For each increment of the global elongation ε, the following relationships must be satisfied:

$$K\varepsilon = \sum_{j=1}^{K} \varepsilon_j \tag{20}$$

and

$$N\sigma(\varepsilon) = \sum_{i=1}^{N_j} \sigma_i(\varepsilon_j), \qquad \text{for} \quad j = 1, 2, \ldots, K \tag{21}$$

In these equations ε_j is the elongation of bundle j (all bundles have equal initial length), $\sigma_i(\varepsilon_j)$ is the tenacity of fibre i in bundle j, and N_j is the number of non-broken fibres in bundle j. Equation (20) just states that the global elongation equals the sum of bundle elongations divided by the number of bundles. The load must be the same at all positions along the chain, and the load balance is expressed by equation (21). Hence, $K+1$ non-linear equations must be solved for each increment of ε, in order to determine the elongations of K bundles and the tenacity of the chain.

The strength (maximum tenacity) of the chain-of-bundles is equal to the strength of its weakest bundle. Before the maximum tenacity is reached, the elongation and tenacity of all bundles increase monotonically. (The tenacity vs. elongation of a bundle or a chain-of-bundles is discontinuous at the elongations at break of each constituent fibre. However, the derivative is always positive when it is finite.) After this, the elongation of the weakest bundle will still increase, while the elongation of all other bundles will decrease. We assume that the stress–strain relationships of the non-broken fibres in these bundles are reversible up to the elongation corresponding to the strength of the chain.

Typical responses of chains with $N = 100$ and various values of K are shown in *Figure 15*. The elongation at break of the chain decreases with increasing K. This is easily understood from equation (20): the elongation of the weakest bundle increases faster than the elongation of the chain. As the tenacity of the chain decreases towards zero, the elongation of the weakest bundle increases towards $K\varepsilon$. In the limit $K \to \infty$, the tenacity of the chain will increase monotonically to its maximum and then fall abruptly to zero. The difference between the elongation at break and the elongation at maximum tenacity of the chain decreases with increasing K as a power law ($\sim K^{-a}$).

The strength of the chain decreases with increasing K, simply because there are more bundles among which to choose the weakest. Hence, the elongation at maximum tenacity will decrease with increasing K as well, since the average tensile response of the bundles is independent of K. Strength vs. K for chains containing FN and FB fibres is shown in *Figure 16*. Note that the strength of the FB chain exceeds that of the FN chain at high K values.

The most important criterion for a weak bundle is that the average tenacity at break of constituent fibres is low. Hence, a weak FN bundle should contain many fibres with high elongation at break, see *Figure 2*. For fibre FB, on the other hand, there is almost no correlation between elongation and tenacity at break, see *Figure 3*. Nevertheless, FB fibres with low or high elongation at break might be preferred in a weak bundle—the former simply because they break before a typical elongation corresponding to maximum bundle tenacity is reached, the latter because their tenacity is still well below their tenacity at break at this typical elongation.

The difference between weak bundles of FN and FB fibres can be illustrated by some data obtained for chains with $N = 10$ and $K = 1000$: average elongation at break of fibres in the weakest bundle is 132% and 118% for FN and FB, respectively. About 50% of these FN fibres have elongation at break above 150%, see *Figure 2*. The

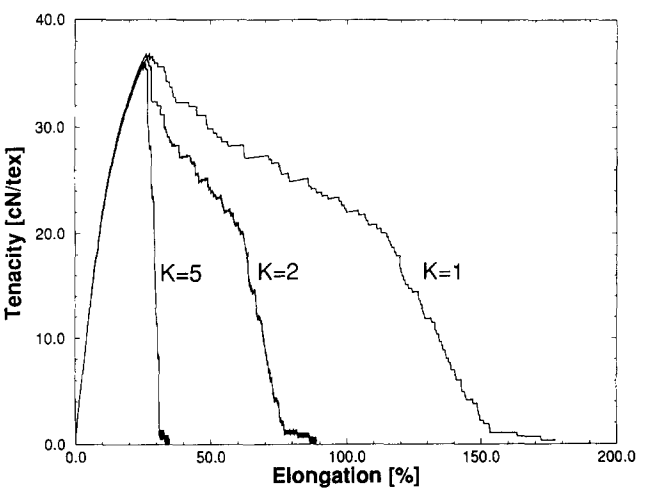

Figure 15 Typical calculated tensile response for the chain-of-bundles model, based on fibre FB. $N = 100$ and $K = 1$, 2 and 5

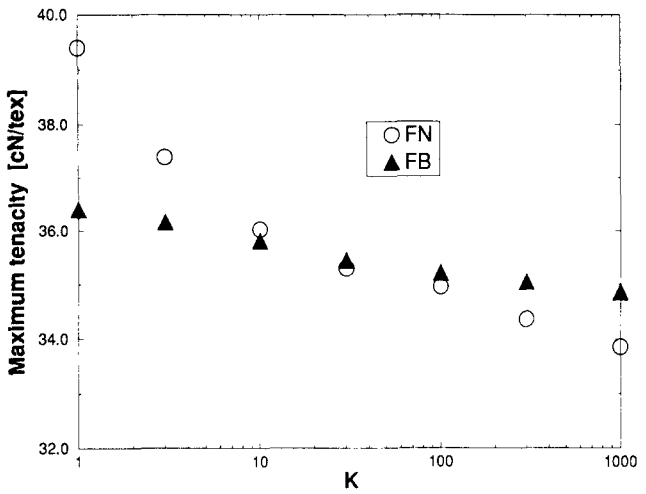

Figure 16 Calculated maximum tenacity for the chain-of-bundles model with $N=100$. Each point is the average of 20–60 simulated chains. Asymptotic values ($N\rightarrow\infty$) calculated by equation (8) are plotted for $K=1$

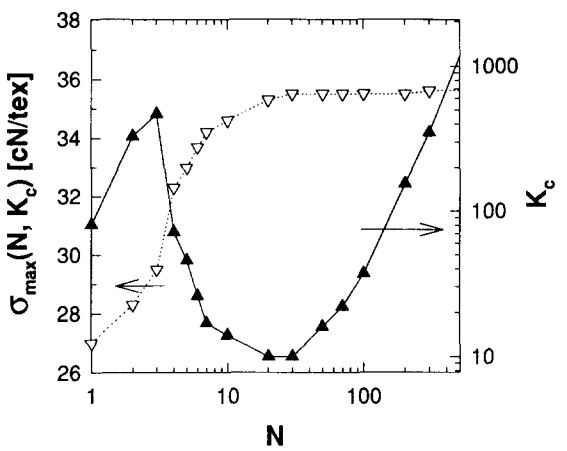

Figure 17 Chain strength and K_c vs. N. The correction factors, $c(\varepsilon)$ (*Figure 6*), are applied to the bundles for $N>1$. The K_c values at low N values (typically 2–5) change if the correction factors are omitted, but the trends remain the same

corresponding average tenacity at break is 42.6 and 35.2 cN tex^{-1}, respectively. The latter is smaller due to a larger 'pool' of fibres with low tenacity at break to select from (*Figure 3*). However, the strength of the FB chain is higher than that of the FN chain, even though the average tenacity at break of the fibres in its weakest bundle is lower. This must be due to the different slopes of the stress–strain curves beyond the yield elongation, see *Figure 1*.

The chain strength also depends on N, the number of fibres in each bundle. In the limit $N\rightarrow\infty$, the strength is independent of K, since all bundles will have the same tensile response. For a given K the strength decreases with decreasing N, since a smaller bundle is more likely to have extreme tensile properties, see *Figure 10*. The difference between FN and FB chains increases with decreasing N: for $K=1000$ the chain strength decreases from 33.9 to 30.1 cN tex^{-1} and from 34.9 to 32.3 cN tex^{-1} for fibres FN and FB, respectively, as N decreases from 100 to 10 (these strengths are average values based on the simulation of 40 chains).

We have seen that the strength of chains decreases monotonically with increasing K and decreasing N, for both types of fibres. However, the K value at which the strength of the FB chain exceeds that of the FN chain (K_c) varies with N, as shown in *Figure 17*. The main effects responsible for the K_c vs. N curve are summarized below.

1. $N=1$. For $N=1$, the chain strengths are directly determined by the low-end tail of the distribution of tenacity at break for single fibres. The tail for fibre FN extends lower. Hence, as K increases, the strength of the FB chain eventually exceeds that of the FN chain.
2. $N\in[1,3]$. In this interval K_c increases with increasing N. This is because the low-end tail of tenacity at break is 'one-dimensional' for fibre FN (*Figure 2*), while it is more or less two-dimensional for the other fibre (*Figure 3*). Hence, fibre FB has a larger pool of weak fibres, and for $K=K_c(N=1)$, the probability of selecting several weak fibres (to make a weak bundle) is higher for type FB, and the FN bundle still has the highest strength at this K value.
3. $N\in[3,25]$. In this interval K_c decreases with increasing N. As N increases, the elongation of the chain at maximum tenacity decreases. A fibre with a given elongation and tenacity at break contributes less to the chain strength (i.e. at low elongations) if it is of type FN, due to the slope of the stress–strain curve (*Figure 1*).
4. $N\in[25,\infty\rangle$. In the limit $N\rightarrow\infty$, the chain strength is independent of K, and the FN chain will be the strongest, as shown in *Figure 7*. Hence, $K_c\rightarrow\infty$ in this limit, and $K_c(N)$ starts increasing at $N=25$. *Figure 17* also shows that the chain strength for a given N and K_c increases asymptotically towards the FB strength in *Figure 7*.

SUMMARY AND CONCLUSIONS

For PP fibres with high draw ratios, the correlation between ε_b and σ_b of the parallels tested is affected by the width of the *MWD*. For broad *MWD* fibres the correlation coefficient is low, while it is close to -1 for narrow *MWD* fibres. A consequence of this is that the latter type of fibre has a broader distribution of σ_b values.

The cumulative distributions of σ_b are adequately described by two-parameter Weibull functions. The cumulative distributions of ε_b differ from this by not having a tail at low ε_b values. Instead it seems to increase as the square root of ε_b. Hence, fracture *PDF*s found in this study have two local maxima.

After a coordinate transformation $(\varepsilon_b,\sigma_b)\rightarrow(\zeta,\xi)$, the fracture *PDF*s for the fibres in this study can be written as a product of two independent functions.

The asymptotic tensile response of a fibre assembly can be calculated by scaling an average stress–strain curve according to the distributions of ε_b and σ_b, in combination with a description of the fibre configuration. By such a calculation, effects of the general shape of the stress–strain curves, and of the distribution of ultimate tensile properties, can be isolated.

The asymptotic responses of bundles of parallel fibres have been calculated for two PP fibres with high draw ratios. The maximum tenacity (strength) of the bundle containing narrow *MWD* fibres is 8% higher than that

of the bundle containing the broad *MWD* fibres, while the average strength of the former fibre type is 29% higher. The ratio of bundle strength to average fibre strength is 77% and 92% for narrow and broad *MWD* fibres, respectively.

Experimental stress–strain curves for fibre bundles deviate somewhat from the calculated curves. This is probably due to different distributions of clamping force on fibres when bundles and single fibres are tested.

A planar distribution of infinitely long fibres can be considered as a reference system for the maximum strength of a non-woven fabric. The ratio of asymptotic strength of a random planar distribution to average fibre strength is 36% and 44%, for the narrow and broad *MWD* fibres in this study, respectively.

The strength of a chain-of-bundles decreases as the number of bundles (K) increases, and as the number of fibres (N) in each bundle decreases. At high K values ($K \geqslant K_c$), the strength of a chain-of-bundles containing broad *MWD* fibres is higher than that of a chain with narrow *MWD* fibres. This effect might also be present in some real fibre assemblies, such as non-woven fabrics. K_c vs. N has two minima.

The description of the stress–strain relationships of constituent fibres, which is used in this article, can be implemented in a microscopic model for a non-woven fabric.

ACKNOWLEDGEMENT

This paper is based on results from the 'Expomat Fibre Project', supported by Borealis and The Research Council of Norway.

REFERENCES

1 Militký, J. and Vaníček, J. *Acta Polym.* 1991, **42**, 326
2 Pompo, A., D'Amore, A., Saiello, S., Nicolais, L., Acierno, D., Bianchi, R. and Vosa, R. *J. Mater. Sci. Lett.* 1992, **11**, 504
3 Amornsakchai, T., Cansfield, D. L. M., Jawad, S. A., Pollard, G. and Ward, I. M. *J. Mater. Sci.* 1993, **28**, 1689
4 Tsai, J.-S. *J. Mater. Sci.* 1993, **28**, 4841
5 Daniels, H. E. *Proc. R. Soc. London Ser. A* 1945, **183**, 405
6 Coleman, B. D. *J. Appl. Phys.* 1957, **28**, 1065
7 Coleman, B. D. *J. Appl. Phys.* 1958, **29**, 968
8 Suh, M. W., Bhattacharyya, B. B. and Grandage, A. *J. Appl. Prob.* 1970, **7**, 712
9 Phoenix, S. L. and Taylor, H. M. *Adv. Appl. Prob.* 1973, **5**, 200
10 Sen, P. K. *J. Appl. Prob.* 1973, **10**, 586
11 Galambos, J. 'The Asymptotic Theory of Extreme Order Statistics', Wiley, New York, 1978
12 Smith, R. L. and Phoenix, S. L. *J. Appl. Mech.* 1981, **48**, 75
13 Sornette, D. *J. Phys. A: Math. Gen.* 1989, **22**, L243
14 Boyce, M. C., Palmer, M. L., Seo, M. H., Schwartz, P. and Backer, S. *J. Appl. Polym. Sci., Appl. Polym. Symp.* 1991, **47**, 383
15 Britton, P. N., Sampson, A. J. and Gettys, W. E. *Text. Res. J.* 1984, **54**, 425
16 Britton, P. N., Sampson, A. J. and Gettys, W. E. *Text. Res. J.* 1984, **54**, 1
17 Britton, P. N., Sampson, A. J., Elliot, C. F., Graben, H. W. and Gettys, W. E. *Text. Res. J.* 1983, **53**, 363
18 Grindstaff, T. H. and Hansen, S. M. *Text. Res. J.* 1986, **56**, 383
19 Andreassen, E., Myhre, O. J., Hinrichsen, E. L. and Grøstad, K. *J. Appl. Polym. Sci.* 1994, **52**, 1505
20 Dimitrova, D., Kostov, G. and Garova, G. *Polymer* 1993, **34**, 4732
21 Lienkamp, M. and Exner, H. E. *Z. Metallkd.* 1993, **84**, 286
22 Samuels, R. J. 'Structured Polymer Properties', Wiley, New York, 1974
23 Kausch, H. H. 'Polymer Fracture', Springer, Berlin, 1978
24 Warner, P. *SPE Annual Technical Conference* 1988, **34**, 1211
25 Wei, K. Y., Vigo, T. L. and Goswami, B. C. *J. Appl. Polym. Sci.* 1985, **30**, 1523
26 Sornette, D. and Redner, S. *J. Phys. A: Math. Gen.* 1989, **22**, L619